

# A robust lower limit on the amplitude of matter fluctuations in the universe from cluster abundance and weak lensing

Rachel Mandelbaum<sup>1,\*</sup> and Uroš Seljak<sup>2,3,4,†</sup>

<sup>1</sup>*Institute for Advanced Study, Einstein Drive, Princeton, NJ 08540, USA*

<sup>2</sup>*Institute for Theoretical Physics, University of Zurich, Zurich Switzerland*

<sup>3</sup>*Department of Physics, Princeton University, Princeton NJ 08544, U.S.A.*

<sup>4</sup>*International Center for Theoretical Physics, Trieste, Italy*

(Dated: October 29, 2018)

Cluster abundance measurements are among the most sensitive probes of the amplitude of matter fluctuations in the universe, which in turn can help constrain other cosmological parameters, like the dark energy equation of state or neutrino mass. However, difficulties in calibrating the relation between the cluster observable and halo mass, and the lack of completeness information, make this technique particularly susceptible to systematic errors. Here we argue that a cluster abundance analysis using statistical weak lensing on the stacked clusters leads to a robust lower limit on the amplitude of fluctuations. The method compares the average weak lensing signal measured around the whole cluster sample to a theoretical prediction, assuming that the clusters occupy the centers of all of the most massive halos above some minimum mass threshold. If the amplitude of fluctuations is below a certain limiting value, there are too few massive clusters in this model and the theoretical prediction falls below the observations. Since any effects that modify the model assumptions can only further decrease the prediction of the model in the context of this method, the limiting amplitude becomes a robust lower limit. Here, we apply it to a volume limited sample of 16,000 group/cluster candidates identified from isolated luminous red galaxies (LRGs) in the Sloan Digital Sky Survey (SDSS). We find  $\sigma_8(\Omega_m/0.25)^{0.5} > 0.62$  at the 95% c.l. after taking into account observational errors in the lensing analysis. While this is a relatively weak constraint, both the scatter in the LRG luminosity-halo mass relation and the lensing errors are large. The constraints could improve considerably in the future with more sophisticated cluster identification algorithms and smaller errors in the lensing analysis. We argue that the existence of a lower limit from cluster abundance is rather general, and demonstrate that Malmquist bias dominates over Eddington bias in this type of analyses.

PACS numbers:

## I. INTRODUCTION

The abundance of clusters of galaxies has been long recognized as potentially one of the most powerful probes of cosmological parameters. The main idea is that the cluster abundance can be related to the abundance of dark matter halos, which are compared to the theoretical halo mass function predictions. These have an exponential cutoff at the high mass end above the so-called nonlinear mass. The nonlinear mass is most sensitive to the amplitude of fluctuations, usually expressed as  $\sigma_8$ , but also depends on other cosmological parameters such as the matter density  $\Omega_m$ . By measuring the cluster abundance evolution with redshift, one can determine the growth rate of structure. Combination with other probes such as the cosmic microwave background, supernovae, and galaxy clustering makes cluster abundance measurement a very powerful probe of such fundamental parameters as neutrino mass and dark energy density [1, 2, 3, 4].

Existing cluster surveys identify clusters based on an

observable property like luminosity. One typically identifies a flux or surface brightness limited sample in a given area based on one of the observables, and follow up observations determine the cluster redshifts via cluster member spectroscopy. With redshift information, volume-limited samples of constant luminosity threshold can be defined, and the cluster volume density determined. In X-ray surveys, the total cluster luminosity is used as an observable [5], although other variables may reduce the scatter [6]. In optical surveys, either cluster richness, total luminosity or central galaxy luminosity is used as the cluster observable [7, 8, 9]. Finally, Sunyaev-Zel'dovich (SZ, [10]) surveys use either the total SZ luminosity or the central decrement. To relate the cluster sample to the halo mass function, one must connect the observable to the halo mass. With X-ray data, the halo mass can be determined from the measurement of X-ray temperature and intensity profile, which allows one to determine the mass profile through the equation of hydrostatic equilibrium. Optical surveys may use velocity dispersion measurements, but recently weak lensing calibration has also become possible [11]. The SZ signal may already be a reliable tracer of the dark matter halo mass, since it is only weakly affected by astrophysical complications like gas cooling, feedback, cosmic rays, etc. [12, 13]. While this technique is still in its infancy, several surveys should

---

\*Electronic address: rmandelb@ias.edu; Hubble Fellow

†Electronic address: seljak@itp.uzh.ch

transform it into reality in the near future.

In all cosmological applications of cluster abundances, an accurate calibration between the observable and dark matter mass is required. It is important not just to determine the mean of this relation (e.g. [14]), but also its scatter [15, 16] and higher moments. Small errors in this calibration may significantly affect the final cosmological parameters. For example, given the steepness of the mass function, a Gaussian scatter brings many more low mass halos into the cluster sample than large mass halos out of the sample, increasing the abundance for a fixed cutoff in the observable. On the other hand, if a cluster is truly dark, it cannot be observed at all, so the cluster sample is incomplete at a given mass threshold, and the observed abundance is below the true value. In general, given the steepness of the mass function, even a small deviation from Gaussianity at the tail of the error distribution can cause a significant effect, which is very difficult to identify with current methods using small subsamples of clusters for which the mass is determined individually.

The second problem in cluster abundance analyses is that some mass determination methods may be unreliable because the assumptions on which they rely may be violated. For example, mass determination from X-ray measurements of gas intensity and temperature using hydrostatic equilibrium assumes that the pressure support is thermal, while additional sources of pressure (cosmic rays, magnetic fields, bulk motions, etc.) are ignored [12, 17]. Other X-ray observables (e.g. the product of the X-ray temperature and the gas mass within  $r_{500}$ , or  $Y_x$ , [6]) may not require the assumption of hydrostatic equilibrium, but still must be calibrated against simulations, which may not include all of the relevant physics. It is generally accepted that gravitational lensing is the most direct tracer of the halo mass, so any attempts at deriving reliable constraints from cluster abundances should ideally be based on lensing.

The third problem is that the calibration between the observable and the halo mass is usually done on a subsample of clusters, which may not be representative. An example is the relation between mass and X-ray luminosity, which is often calibrated on relaxed clusters for which the hydrostatic equilibrium assumption may be valid, while the results are then applied to the whole cluster sample even though non-relaxed clusters may not obey this relation.

These arguments suggest that only if clusters are identified by mass selection, such as when using the dark matter maps derived from gravitational lensing, can one avoid these potential systematic errors. Unfortunately, mass selection of clusters is still far away from being practically implemented. Also, while in principle a mass-selected sample lacks the difficulties of the current methods, the amount of cosmological information is limited without redshift information. If the redshift is sought afterwards, there is again the possibility that the selected cluster candidate lacks bright galaxies, bringing in astrophysical complications. Moreover, there is considerable

scatter between the halo mass derived from lensing and the more traditional halo mass estimates [18]. For example, in some cases this mass selection may result in a random superpositions of filaments rather than true virialized clusters, so one must be able to quantify the rate of such occurrences. Alternatively, several promising self-calibration methods were proposed for future large data sets [19, 20], and in some cases were already applied to existing data sets [7], but it remains to be seen whether these methods can reliably solve all of the aforementioned problems.

It is worth asking if there is any robust information that can be extracted from the cluster abundances without making additional assumptions that increase the susceptibility to hidden systematic errors. We have established above that to derive a robust constraint, we must use gravitational lensing to relate the observable to mass; that this analysis should use the complete sample of clusters; and that the effects of scatter and incompleteness are difficult to fully account for. Here, we propose a method that uses lensing analysis on the entire cluster sample. Because the issues of completeness and scatter cannot be fully solved without additional assumptions, only an inequality can be established.

We propose the following analysis. Given a cluster sample with a known number density at a given redshift, we compute the halo mass function for a given cosmology (i.e., amplitude of fluctuations assuming a value for  $\Omega_m$  and other cosmological parameters). From this, we can compute the theoretical prediction for the mean weak lensing signal around the clusters assuming that the cluster positions are at the centers of all of the most massive halos predicted by the model (with a minimum halo mass  $M_{min}$  determined by the cluster abundance). This is the maximally allowed lensing signal for that cosmological model, since placing the clusters at any other position can only lower the lensing prediction. From the data, one can compute the mean weak lensing signal around the clusters by stacking the individual signals. Stacking reduces the noise, so that the resulting  $S/N$  can be high even if it is low from an individual cluster. Furthermore, it avoids the problems with individual cluster lensing mass determination mentioned in [18], since we only require that the stacked signal give information about the cluster mass in the mean. As in [21], comparison with N-body simulations suggests that this assumption is valid.

This signal can then be compared to the theoretical predictions. These depend mostly on the amplitude of fluctuations: lowering it will reduce the number of high mass clusters and the lensing signal amplitude. At some point the theoretical predictions fall below the observations. Such a cosmological model cannot be allowed, since any failure of the assumption that the cluster sample corresponds to the centers of the most massive halos can only reduce the lensing signal, making the discrepancy worse. The amplitude of fluctuations for which the theoretical prediction still matches the observations

within the observational errors is thus a robust lower limit.

This method can be applied to any cluster sample, no matter how incomplete, but the derived lower limit improves if the sample is closer to the complete sample of most massive halos. This may be a small effect if one is on the exponential tail, where a small change in amplitude causes a large change in the abundance. Note that within the context of this method, we cannot establish when the inequality becomes equality. This would require an assessment of completeness and scatter in the observable-mass relation, which as argued above is very difficult and may not even be possible if some of the clusters are truly dark.

In this paper, we apply the method to a cluster sample derived from isolated luminous red galaxies (LRGs) in Sloan Digital Sky Survey (SDSS), for which the high signal to noise of the lensing signal has already been established [9]. The advantages of this sample are that it covers an unprecedentedly large volume and is essentially volume limited. On the other hand, the LRG luminosity is unlikely to be a perfect tracer of cluster mass, so with a better tracer the constraints may be improved in the future (for example using the maxBCG cluster sample presented in [22]).

Here we note the cosmological model and units used in this paper. All data-related computations assume a flat  $\Lambda$ CDM universe, though  $\Omega_m$  itself is allowed to vary. Distances quoted for transverse lens-source separation are comoving (rather than physical)  $h^{-1}$ kpc, where  $H_0 = 100 h \text{ kms}^{-1} \text{ Mpc}^{-1}$ . Likewise,  $\Delta\Sigma$  is computed using the expression for  $\Sigma_c^{-1}$  in comoving coordinates, where  $\Sigma_c$  is the critical surface density that depends on the distance ratios [9]. For the typical lens and source redshifts in this study,  $\Sigma_c$  depends on cosmology only at the 0.1% level even for extreme changes in cosmology. In the distance units used,  $H_0$  scales out of everything, so our results are independent of this quantity. When masses are quoted in  $M_\odot$  rather than  $h^{-1}M_\odot$ , we have used  $h = 0.7$ .

## II. DATA SAMPLE AND ANALYSIS

As the basis of the cluster sample we use the spectroscopic sample of LRGs from the latest release of SDSS, data release 5 [23, 24]. These are good tracers of massive halos, as suggested by their large bias [25]. Previous lensing analyses [9] have established that the minimum halo mass is  $\sim 5 \times 10^{13} M_\odot$  and that there is a correlation between LRG luminosity and halo mass,  $M \propto L^2$ , for masses up to  $2 \times 10^{14} M_\odot$ . The complete, approximately volume-limited sample consists of  $\sim 40,000$  galaxies with  $0.15 < z < 0.35$  and a comoving volume of  $0.44(\text{Gpc}/h)^3$ . We identify a higher-luminosity subsample of host LRGs using spectroscopic galaxy counts in cylinders of comoving radius  $1 h^{-1} \text{ Mpc}$  and line-of-sight length  $\Delta v = \pm 1200 \text{ km s}^{-1}$ . Since we only want to elimi-

nate galaxies for which there is another, brighter spectroscopic LRG nearby, we simply require that the LRGs in our sample either (a) be the only one in the cylinder centered on its position, or (b) be the brightest in the cylinder. This cut, which is weaker than the overly-stringent cut in [9] using a  $2 h^{-1} \text{ Mpc}$  cylinder radius, eliminates about 7.5% (rather than 13%) of the complete sample.

For the LRG luminosity, we use  $r$ -band model magnitudes  $k + e$ -corrected to  $z = 0$  as in [9] to create luminosity-threshold samples with  $M_r < -22.3$ ,  $< -22.6$ , and  $< -23$  containing 15 635, 5 099, and 902 galaxies (respectively). Because of scatter in  $M(L)$ , there is no guarantee that this will have the desirable effect of selecting the most massive among the halos in the sample.

LRGs targeted for deeper spectroscopy in SDSS have a very specific color selection [26], and it is unlikely that only the galaxies that satisfy the LRG criteria can be central galaxies in clusters above our mass threshold. Indeed, in [22], only 70% of SDSS maxBCG clusters in regions with spectroscopy contain LRGs with spectra. We quantify the effects of color-related incompleteness using a comparison against the SDSS Main galaxy sample, which is purely flux-limited at a brighter limiting flux. The highest luminosity sample from our previous Main sample lensing analyses [27], with Petrosian  $r$ -band magnitude  $k$ -corrected to  $z = 0.1$  satisfying  $-22 \geq M_r > -23$  (the L6 sample), overlaps significantly with the spectroscopic LRG sample in redshift, and thus is an ideal sample for quantifying the effects of the LRG color cut. LRGs constitute 65% of this brightest Main subsample, so one possibility is to supplement the LRGs with the galaxies that are equally as bright but not as red. The Main sample limiting apparent magnitude is 17.77, so these L6 galaxies appear significantly brighter than the complete LRG sample ( $r < 19.1$ ), partially because their maximum redshift is lower ( $\sim 0.25$  rather than 0.35). However, their lensing-weighted mean redshift,  $\langle z \rangle = 0.2$ , is not that different from that of the LRG sample,  $\langle z \rangle = 0.24$ , because lensing gives the highest signal for the galaxies that are halfway between  $z = 0$  and the sources at redshift 0.3-0.6. The L6 Main sample galaxies were split into the 65% that pass the LRG selection and the remaining 35% that fails it.

As shown in figure 1, weak lensing analysis reveals that halos of the non-LRG L6 galaxies are  $(30 \pm 20)\%$  less massive on average. The masses were derived from NFW ([28]) fits to the inner  $0.5 h^{-1} \text{ Mpc}$  with fixed concentration  $c = 6$ , where host group/cluster contributions for satellite lenses are negligible (since we do not have a reliable environment estimator for L6 that will allow us to remove satellite galaxies as we do for the LRGs). The reduced  $\chi^2$  values for these fits are 0.53 (non-LRGs) and 1.0 (LRGs), which suggests that the NFW model is an acceptable description of the data (particularly when accounting for the increase in  $\chi^2$  due to noise in the jackknife covariance matrices, [38]). Unlike in [9], the virial radius in this case is defined as the radius within which

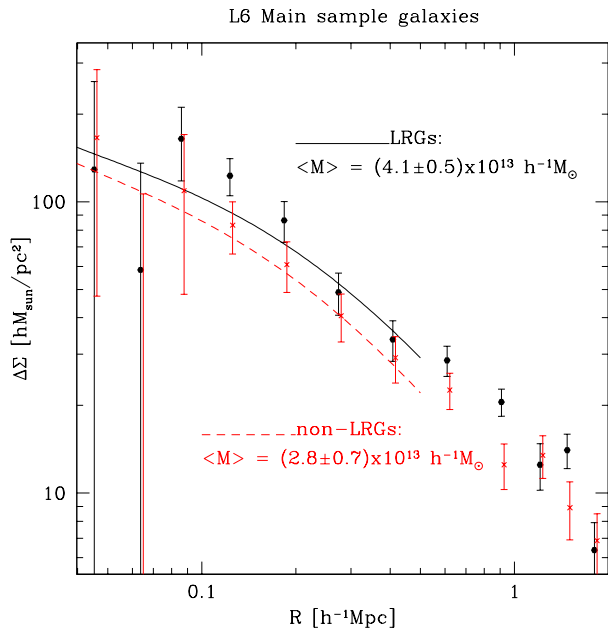


FIG. 1: The lensing signal for the brightest Main sample galaxies, divided into those that are spectroscopic LRGs and those that are not. We also show the best-fit lensing signal on small scales (where the contribution due to host halos for those that are satellites is small), giving average estimated virial halo masses using the methodology of [9].

the average halo density is  $280\bar{\rho}$ . Allowing the concentration to vary lessens the difference to  $\sim 10\%$ , as the best-fit concentration for the L6 LRG sample is higher than that of the L6 non-LRG sample. It is important to note that these non-LRG L6 galaxies are on average  $\sim 0.1$  mag fainter than L6 LRGs. Given that we have previously established  $M \propto L^2$  at the high-luminosity end [9], we would indeed expect the L6 non-LRGs to be 20% less massive. Within the errors, these results therefore justify our assumption that non-LRG galaxies are in equally massive halos as LRG galaxies of the same luminosity in  $r$ . Thus, we increase the number density of LRGs by 38% for  $M_r < -22.3$ , and 25% for  $M_r < -22.6$  and  $M_r < -23$  according to the fractions of L6 galaxies that are classified as LRGs in these bins. We use these increased abundances (including the correction for the overly-stringent satellite cut described previously) in this paper while analyzing the LRG sample signal presented in [9]. The abundance corrections due to the satellite cut vary based on LRG luminosity, and lead to an increase of 7.5% in the abundance of the complete sample, or 6.0%, 2.6%, and 0.7% for the three luminosity threshold samples.

The weak lensing analysis is the same as in [9]. More than 30 million source galaxies are identified, their shape measurements obtained using the Reglens pipeline, including PSF correction done via re-Gaussianization [29] and with cuts designed to avoid various shear calibration biases. A full description of this pipeline can be

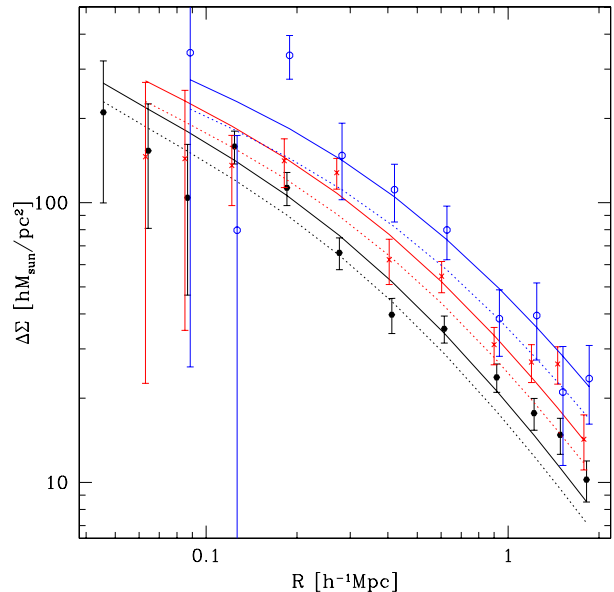


FIG. 2: The lensing signal for the spectroscopic LRGs in luminosity threshold samples,  $M_r < -22.3$  (black hexagons),  $< -22.6$  (red crosses), and  $< -23$  (blue circles). Bootstrap  $1\sigma$  errors are shown, along with the theoretical signal for the best-fit  $\sigma_8$  with  $\Omega_m = 0.25$  (fixed) as a solid line, and the 95% CL lower limit as a dotted line.

found in [30]. The main difference relative to that paper is that the results of the Shear TESTING Programme (STEP) comparison to simulations are now available and suggest that Reglens is well calibrated at the 2% level [31]. Our redshift distributions are calibrated using the DEEP2 spectroscopic survey [30, 32]. As in [30], we assume a total 8% calibration uncertainty ( $1\sigma$ ), though this is likely to be a conservative estimate.

Since we know the LRG lens redshifts, we can express the lensing signal in terms of the differential surface mass density  $\Delta\Sigma$  as a function of transverse separation  $R$ . We average the signal over all the clusters, so the result is the average weak lensing profile around them. Our lensing signal estimator, with all associated tests and corrections (for imperfect sky subtraction, intrinsic alignments, non-weak shear, and other effects), is described in detail in [9]. The results are shown in figure 2 for various luminosity threshold subsamples. We see that the signal increases with luminosity, so the luminosity thresholds do have the desirable effect of preferentially selecting more massive halos. We also see that the signal is inconsistent with zero at several standard deviations for all luminosity threshold samples and transverse separations shown in the figure. The total  $S/N$  (over all transverse separations using the full jackknife covariance matrix) is 19, 17, and 11 for the  $M_r < -22.3$ ,  $< -22.6$ , and  $< -23$  threshold samples respectively.

### III. RESULTS

We want to compare the weak lensing signal to a theoretical prediction under the assumption that all of the most massive halos have been occupied. We use the Sheth and Tormen halo mass function [33], but with parameters as suggested in [34] and defining the halo mass using the radius within which the average density is  $280\bar{\rho}$ . These two choices represent departures from the analysis in [9]. The halo mass function specifies the number density of halos as a function of mass,  $dn/dM$ . For each luminosity threshold we select the minimum mass such that the integrated number density equals the observed one,  $\int_{M_{\min}}^{\infty} (dn/dM)dM = n_0$ , where  $n_0$  is 5.20, 1.48, and  $0.26 \times 10^{-5} (h/\text{Mpc})^3$  for the three luminosity threshold subsamples (with  $\Omega_m = 0.25$ ).

Once we have the minimum mass, we compute the prediction for the weak lensing signal,

$$\langle \Delta\Sigma \rangle = \frac{1}{n_0} \int_{M_{\min}}^{\infty} \frac{dn}{dM} \Delta\Sigma(M) dM, \quad (1)$$

where  $\Delta\Sigma(M)$  is the differential surface density for a cluster of mass  $M$ , which we model as an NFW profile with concentration parameter that depends on the nonlinear mass and which must be calculated for each cosmology separately using  $c(M) = 10(M/M_{\text{nl}})^{-0.13}$  [35]. Here  $M_{\text{nl}}$  is the nonlinear mass, defined as the mass in a sphere within which the rms overdensity fluctuation is 1.68. The concentration dependence on the cosmological model mildly enhances the scaling with amplitude, because in a model with a lower amplitude of fluctuations, not only will  $M_{\min}$  at a given abundance be lower, but so will be concentration, which reduces the signal at scales smaller than the virial radius. As in our previous analysis with this sample, we include a stellar component with mass and radius that is fixed to a value determined from the optical luminosity. This component is important for  $0.04 < R < 0.08h^{-1}\text{Mpc}$ , a small fraction of the region used for the fits ( $0.04 < R < 2h^{-1}\text{Mpc}$ ).

This calculation is done separately for each cosmology. For the mass function, the most important parameter is the nonlinear mass, which depends on the amplitude of fluctuations  $\sigma_8$  and mass density  $\Omega_m$ . For  $\sigma_8 = 0.75$ ,  $\Omega_m = 0.25$ ,  $z = 0.24$ ,  $n_s = 1$ , and  $h = 0.7$ , figure 3 shows the effect of changing these cosmological parameters on our chosen mass function and confirms the dominant importance of  $\sigma_8$  and  $\Omega_m$ . The shape of the power spectrum also enters the mass function calculation [36], but the variation in the mass function (figure 3) is small given the current uncertainties on the shape of the power spectrum. For example, the change in the mass function is three times smaller for  $n_s$  than for  $\Omega_m$  when using WMAP3, supernovae, galaxy clustering, and Lyman- $\alpha$  forest, [37]. Our use of  $n_s = 1$  gives conservative bounds on  $\sigma_8$ , in the sense that decreasing it by 4% to the value from WMAP3 would decrease the expected abundances by that amount, increasing the best-fit  $\sigma_8$  by  $\sim 2\%$ . Because it is approximately degenerate with  $\Omega_m$  for  $M < 10^{14}h^{-1}M_{\odot}$ , for the

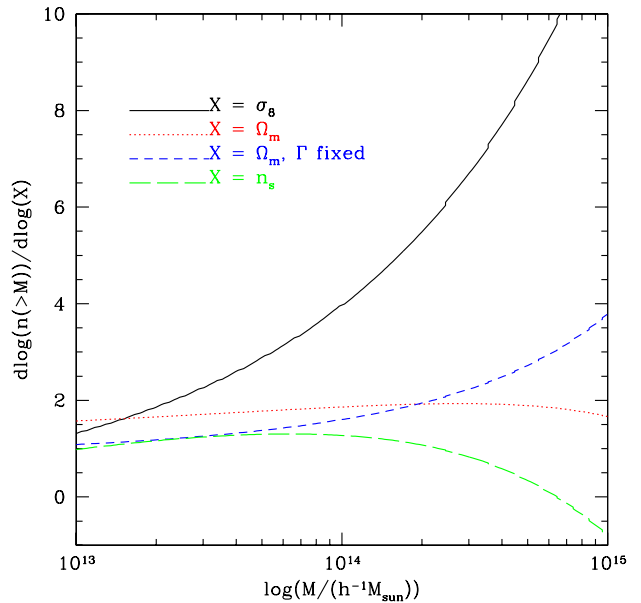


FIG. 3: Parameter dependence of the mass function at the LRG mean redshift for the fiducial cosmology described in the text.

fainter threshold samples where those halo masses dominate, one can estimate the best-fit  $\sigma_8$  for a 4% lower  $n_s$  by simply lowering the fiducial  $\Omega_m$  by that amount instead.

Since we fix  $h = 0.7$ , we effectively have a different power spectrum shape for each value of  $\Omega_m$ , but as shown in the figure, the effect of  $\Omega_m$  on the nonlinear mass definition is the main source of our sensitivity to this parameter, so the curves of variable  $\Omega_m$  with and without fixing the shape parameter  $\Gamma = \Omega_m h$  are similar. Since the matter density affects a number of quantities such as the calculation of distances and volumes, the change in growth factor from  $z = 0.24$  to  $z = 0$ , and the definition of virial radius, we perform the analysis separately for three values,  $\Omega_m = 0.20, 0.25, 0.30$ . For each value of  $\Omega_m$ , we vary only  $\sigma_8$  while fixing the remaining parameters.

We perform the analysis using  $\chi^2$  minimization with respect to  $\sigma_8$ . If  $\sigma_8$  is high, then we will have many high mass halos, so the predicted lensing signal will exceed the observed one. Since deviation from the assumption that all of the most massive halos are in our sample can only reduce the signal, such a model cannot be excluded. Lowering the amplitude of fluctuations reduces the number density of massive halos, so the lensing signal prediction decreases. As a result, there is a value that fits the data best. Reducing the amplitude further drops the model predictions below the observations, so such a model cannot be resurrected. Figure 2 shows the results of this fitting procedure, showing that we can obtain a good fit for each luminosity threshold. The best-fit reduced  $\chi^2$  values for each luminosity threshold are 1.4, 1.2, and 1.2 from faintest to brightest. Accounting for the noise in the

covariance matrix, these  $\chi^2$  values give a  $p(> \chi^2)$  (probability to exceed the  $\chi^2$  value by chance if the model is a good description of the data) of 20%, 40%, and 40%. We also show the prediction of a model which is excluded at the 95% confidence level.

To determine errors on the lensing signal, we divide the survey area into 200 bootstrap subregions, and generate 2500 bootstrap-resampled datasets. We repeat the analysis for each resampled dataset, introducing the 8% systematic calibration uncertainty at this stage. The final outcome of our analysis is a probability distribution for  $\sigma_8$  for each luminosity threshold. This procedure avoids the problems [38, 39] of overly-optimistic parameter constraints due to noise in the bootstrap covariance matrix which tends to increase the fit  $\chi^2$  so it deviates from the usual distribution, and leads to broader parameter distributions than we would have obtained by naively using  $\Delta\chi^2$  values to find confidence regions. The distributions are plotted on figure 4 for  $\Omega_m = 0.25$ . We see that the luminosity thresholds  $M_r < -22.3$  and  $< -22.6$  give the strongest constraints on  $\sigma_8$ , while for  $M_r < -23$  the constraints weaken. If we had a complete sample with no scatter then we should get the same constraints for all the samples (assuming the effects from cosmological parameters besides amplitude are negligible), so the weaker constraints at the bright end suggest that the relation between LRG luminosity and halo mass breaks down there.

We then repeat the analysis for other values of  $\Omega_m$ , covering the range between 0.2 and 0.3. We find that we can match the probability distributions by introducing a variable  $\sigma_8(\Omega_m/0.25)^{0.5}$ . The final outcome from our analysis is thus the probability distribution on this parameter. The constraints can be expressed as  $\sigma_8(\Omega_m/0.25)^{0.5} > 0.68$  at 50% c.l.,  $\sigma_8(\Omega_m/0.25)^{0.5} > 0.62$  at 95% c.l., and  $\sigma_8(\Omega_m/0.25)^{0.5} > 0.60$  at 99% c.l. These constraints are for the largest sample,  $M_r < -22.3$ ; we tried the analysis for the smaller subsamples in case splitting the sample to reach a higher mass threshold would give superior results, but unfortunately this was not the case. These constraints can be easily implemented in Markov Chain Monte Carlo codes when doing global parameter estimates in the form of a soft boundary on this parameter combination. For the median value of  $\sigma_8$  for  $\Omega_m = 0.25$ , the minimum mass thresholds for the  $M_r < -22.3$ ,  $< -22.6$ , and  $< -23$  samples are 3.3, 6.9, and  $14.1 \times 10^{13} h^{-1} M_\odot$ , respectively.

The sources of error for the galaxy-galaxy weak lensing analysis have been discussed in the previous section and are described in more detail in [30], and the overall calibration uncertainty of 8% has been applied to obtain the final results. Similarly, the errors associated with the cluster abundance are described in the previous section, and while we apply a correction for the clusters missed by the LRG selection, this is correction justified by our lensing analysis of Main sample luminous galaxies. One source of error that we likely do not need to worry about is the sampling variance, given that we work with a vol-

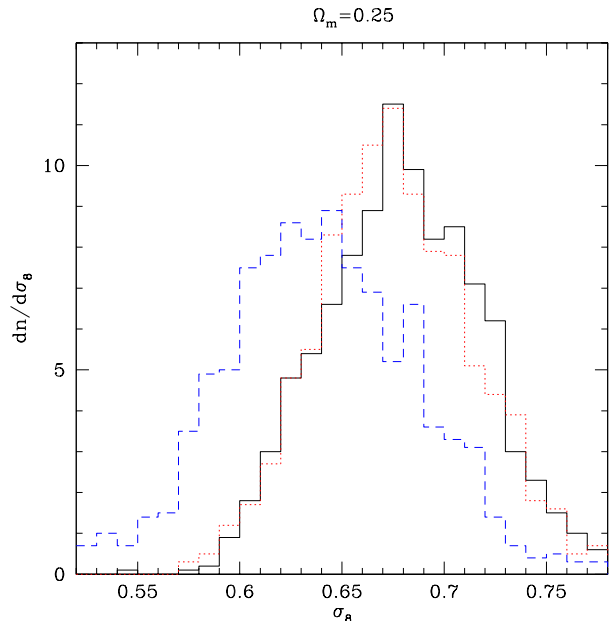


FIG. 4: The distribution of best-fit  $\sigma_8$  values in the bootstrap subsamples assuming fixed  $\Omega_m = 0.25$ , for the three luminosity threshold samples:  $M_r < -22.3$  (black, solid);  $< -22.6$  (red, dotted);  $< -23$  (blue, dashed). Each value should be interpreted as a lower limit due to the failure of modeling assumptions. We see that the brightest sample gives the weakest limits, suggesting that luminosity fails to trace the halo mass with low scatter at the bright end.

ume of about a cubic Gpc with of order 10,000 clusters. For simplicity, we quote the constraint at  $z = 0$ , but the actual constraint is at  $z = 0.24$ , and for a given value of  $\Omega_m$ , we have translated between the two using a  $\Lambda$ CDM cosmological model. To translate to a different model, for example one with dark energy equation of state  $w$  different from  $-1$ , one must multiply by the ratio of the growth factors between these two redshifts for the two models. Over the range of  $w$  allowed by the current constraints and the range of redshifts of concern, these effects are well below the current level of statistical precision.

#### IV. DISCUSSION

We have presented a method that can robustly determine a lower limit to the amplitude of fluctuations in the universe. The method consists of a statistical weak lensing analysis on a stacked cluster sample compared with theoretical predictions, assuming that the sample occupies the centers of all of the most massive halos for that model. The method does not attempt to establish a mass estimate for each cluster, and is thus significantly less observationally demanding than the traditional methods of calibration based on a large cluster subsample for which the mass-observable relation is determined. As a result, only an inequality can be established. On the other hand,

unlike other methods, this method uses mass information extracted from lensing on the complete cluster sample, removing one of the major uncertainties in the traditional approach. Furthermore, the main difficulties in the traditional analyses (knowledge of incompleteness and scatter in the mass-observable relation) are removed when attempting to place only a lower limit. We have applied the method to a sample of 16,000 cluster candidates from SDSS. We find  $\sigma_8(\Omega_m/0.25)^{0.5} > 0.68$  at 50% confidence level and  $\sigma_8(\Omega_m/0.25)^{0.5} > 0.62$  at 95% c.l., where the error is entirely due to statistical and systematic errors in the lensing analysis, while all modeling uncertainties have been absorbed by the inequality.

At first, it appears surprising that a cluster abundance analysis gives a robust lower limit. One effect of scatter in the mass-observable relation relative to no scatter is to increase the number of clusters at a given observable threshold, since for a symmetric error distribution around the mean, there are always more low mass clusters that scatter into the sample than high mass clusters that scatter out of the sample, a consequence of the steepness of the halo mass function. This increase in abundance is the so-called Eddington bias. Ignoring the scatter, one would therefore conclude that the derived value of  $\sigma_8$  is higher than the true value. Consequently, one sometimes finds statements that, ignoring scatter, the cluster abundance gives an upper limit on  $\sigma_8$  [11, 40].

However, such statements are only valid if the relation between the mass and observable is extracted from a complete (or at least unbiased) sample of halos at a given *halo mass* threshold. In practice, for a given sample (whether flux- or volume-limited), this goal is impossible because of scatter: we must define the sample used to determine the mass observable-relation with a given *observable* threshold. Consequently, low mass halos for which the observable is above the mean will be scattered in, and high mass halos for which the observable is below the mean will be scattered out. Since there are more of the former than of the latter due to the declining mass function, the derived mean halo mass at a given observable will be underestimated. This is the Malmquist bias effect that acts in the opposite direction to the Eddington bias, and leads to an underestimate of  $\sigma_8$  [41]. Note that Malmquist bias is present for both flux-limited and volume-limited samples, since the latter are always derived from the former using redshift information. While the two effects oppose each other, our results suggest that the Malmquist bias always dominates, so that only a robust lower limit can be established. We present an analytical derivation of this result in Appendix A. This result should be valid for other cluster abundance analyses where the effects of scatter are not explicitly taken into account, as long as the halo mass determination is reliable (and as long as the sample itself is used to determine the mass-observable relation, rather than simulations). In practice, mass determination may not be reliable for those mass estimates that are not based on lensing, so one cannot conclude that all of the derived

limits from cluster abundance with no attempt to correct for scatter should be interpreted as robust lower limits. Nonetheless, it is clear that scatter is a serious problem, and that it can lead to the opposite effect on  $\sigma_8$  from what is often assumed.

Our lower limit on  $\sigma_8$  is relatively weak, even in the context of the WMAP3 results, which suggest a low amplitude of fluctuations,  $\sigma_8 \sim 0.75$  [42], compared to previous analyses giving 0.9 [43]. The cosmological constraints we find here are likely to be improved further with better cluster samples. First, the errors in the lensing analysis are significant, and the 95% limit is 0.06 lower in  $\sigma_8$  than the median 50% value, so a larger cluster sample or a deeper survey with more background galaxies would reduce the statistical error. Second, in our analysis we work with relatively low mass clusters around  $10^{14}M_\odot$  and densities between  $10^{-5}$  and  $10^{-4}(h/\text{Mpc})^3$ . While the mass function is sensitive to the amplitude of fluctuations in this range, the sensitivity increases as one moves to higher mass clusters with lower number densities, where the mass function exponentially decreases, as shown in figure 3. Third, using isolated LRG luminosity as a proxy for cluster mass is rather unsophisticated. While a relation between the halo mass and LRG luminosity has been established over the range of masses between  $5 \times 10^{13}M_\odot$  and  $2 \times 10^{14}M_\odot$ , it breaks down above that [9], so one cannot use this method to identify a sample of very massive clusters in SDSS. While the scatter between LRG luminosity and halo mass has not been established, it is likely to be significant. Consequently, it is unlikely that the value of the amplitude of fluctuations derived in this paper is very close to the true value. In Appendix A we derive the amplitude of the effect assuming a simple lognormal scatter. The bottom panel of figure 5 shows that for a 50% scatter in the mass-observable relation, the underestimate of  $\sigma_8$  is 6-7%, relatively independent of the mass above  $10^{14}h^{-1}M_\odot$ . However, the scatter can be even larger and may not follow the simple lognormal model. For example, if we apply corrections to the observed lensing signal consistent with the results for the brightest luminosity sample in [21] to account for the effects of scatter in  $M(L)$ , the best-fit values of  $\sigma_8$  changes by 15%. We do not suggest that the model for  $M(L)$  scatter used in that work is a close enough approximation to the real one that this correction should be applied; rather, we include this information to make it very clear that scatter is an important issue for the SDSS LRG sample that can seriously affect measured cosmological parameters.

In the future, it would be worth repeating this analysis on samples of clusters with an even lower number density, for which the abundance is more sensitive to the amplitude of fluctuations. While the number of clusters will be lower, their lensing signal will be higher, so as long as the signal to noise remains high, such analysis will yield useful constraints that may improve upon the ones established in this paper. Many sophisticated algorithms have been developed to select clusters and deter-

mine their mass based on their richness of red galaxies with photometric redshifts [44]. A particularly promising method in the context of the SDSS is MaxBCG [8], which identifies clusters by their concentration of galaxies along the red galaxy color-redshift relation and establishes the mass-richness relation across a broader range of halo mass. We expect that applying our method to this and other samples of clusters will yield lower limits on the amplitude that may be a useful complement to the traditional analyses of cluster abundances which yield very small formal errors, but may contain hidden systematic errors.

Another possibility is to apply this method to the sample of regular  $L_*$  galaxies, tracing halo masses around  $10^{12}M_\odot$ . These galaxies are well below the nonlinear mass, in the regime where the halo mass function is sensitive mostly to  $\Omega_m(n_{\text{eff}} + 3)$ , where  $n_{\text{eff}}$  is the effective slope of the power spectrum at megaparsec scales [45]. Here again only a lower limit to this combination can be established. However, the errors on these parameters from other probes are already quite small, and it is not clear that such analysis would be competitive given the current errors in the lensing analysis.

Is it possible that ultimately the lower limit we es-

tablished here is all that will be achievable with cluster abundance studies, even when a reliable mass tracer such as weak lensing is used? This would be a major retreat compared to the expectations for future surveys [1, 2, 3]. In principle this option cannot be discarded, since there is always a possibility that a subset of dark matter halos is not detected with X-ray, optical or SZ surveys. More generally, the conditional probability distribution of halo mass at a given luminosity may be complicated and difficult to establish using subsamples of data. While it is likely that further studies, both theoretical and observational, will improve our knowledge, the ultimate limitations of the method are difficult to establish. It is therefore important to know that at least some cosmological information extracted from cluster abundance is robust, even if it is only in a form of inequality.

We thank Chris Hirata for numerous discussions. R.M. is supported by NASA through Hubble Fellowship grant #HST-HF-01199.02-A awarded by the Space Telescope Science Institute, which is operated by the Association of Universities for Research in Astronomy, Inc., for NASA, under contract NAS 5-26555. U.S. is supported by the Packard Foundation and NSF CAREER-0132953.

- 
- [1] Z. Haiman, J. J. Mohr, and G. P. Holder, *Astrophys. J.* **553**, 545 (2001).
- [2] J. Weller and R. A. Battye, *New Astronomy Review* **47**, 775 (2003).
- [3] S. Wang, Z. Haiman, W. Hu, J. Khoury, and M. May, *Physical Review Letters* **95**, 011302 (2005), astro-ph/0505390.
- [4] A. Albrecht, G. Bernstein, R. Cahn, W. L. Freedman, J. Hewitt, W. Hu, J. Huth, M. Kamionkowski, E. W. Kolb, L. Knox, et al., *ArXiv Astrophysics e-prints* (2006), astro-ph/0609591.
- [5] Z. Haiman, S. Allen, N. Bahcall, M. Bautz, H. Boehringer, S. Borgani, G. Bryan, B. Cabrera, C. Canizares, O. Citterio, et al., *ArXiv Astrophysics e-prints* (2005), astro-ph/0507013.
- [6] A. V. Kravtsov, A. Vikhlinin, and D. Nagai, *Astrophys. J.* **650**, 128 (2006), astro-ph/0603205.
- [7] M. D. Gladders, H. K. C. Yee, S. Majumdar, L. F. Barrientos, H. Hoekstra, P. B. Hall, and L. Infante, *Astrophys. J.* **655**, 128 (2007).
- [8] B. P. Koester, T. A. McKay, J. Annis, R. H. Wechsler, A. E. Evrard, E. Rozo, L. Bleem, E. S. Sheldon, and D. Johnston, *ArXiv Astrophysics e-prints* (2007), astro-ph/0701268.
- [9] R. Mandelbaum, U. Seljak, R. J. Cool, M. Blanton, C. M. Hirata, and J. Brinkmann, *Mon. Not. R. Astron. Soc.* **372**, 758 (2006), astro-ph/0605476.
- [10] R. A. Sunyaev and Y. B. Zeldovich, *Comments on Astrophysics and Space Physics* **4**, 173 (1972).
- [11] H. Dahle, *Astrophys. J.* **653**, 954 (2006), astro-ph/0608480.
- [12] C. Frommer, T. A. Ensslin, V. Springel, M. Jubelgas, and K. Dolag, *ArXiv Astrophysics e-prints* (2006), astro-ph/0611037.
- [13] E. J. Hallman, P. M. Motl, J. O. Burns, and M. L. Norman, *Astrophys. J.* **648**, 852 (2006), astro-ph/0509460.
- [14] M. R. Francis, R. Bean, and A. Kosowsky, *Journal of Cosmology and Astro-Particle Physics* **12**, 1 (2005), astro-ph/0511161.
- [15] E. S. Levine, A. E. Schulz, and M. White, *Astrophys. J.* **577**, 569 (2002), astro-ph/0204273.
- [16] M. Lima and W. Hu, *Phys. Rev. D* **72**, 043006 (2005), astro-ph/0503363.
- [17] E. Rasia, S. Ettori, L. Moscardini, P. Mazzotta, S. Borgani, K. Dolag, G. Tormen, L. M. Cheng, and A. Diaferio, *Mon. Not. R. Astron. Soc.* **369**, 2013 (2006), astro-ph/0602434.
- [18] C. A. Metzler, M. White, and C. Loken, *Astrophys. J.* **547**, 560 (2001).
- [19] W. Hu, *Phys. Rev. D* **67**, 081304 (2003), astro-ph/0301416.
- [20] S. Majumdar and J. J. Mohr, *Astrophys. J.* **613**, 41 (2004), astro-ph/0305341.
- [21] R. Mandelbaum, A. Tasitsiomi, U. Seljak, A. V. Kravtsov, and R. H. Wechsler, *Mon. Not. R. Astron. Soc.* **362**, 1451 (2005), astro-ph/0410711.
- [22] B. P. Koester, T. A. McKay, J. Annis, R. H. Wechsler, A. Evrard, L. Bleem, M. Becker, D. Johnston, E. Sheldon, R. Nichol, et al., *ArXiv Astrophysics e-prints* (2007), astro-ph/0701265.
- [23] D. G. York, J. Adelman, J. E. Anderson, S. F. Anderson, J. Annis, N. A. Bahcall, J. A. Bakken, R. Barkhouser, S. Bastian, E. Berman, et al., *Astron. J.* **120**, 1579 (2000).
- [24] J. K. Adelman-McCarthy, M. A. Agüeros, S. S. Allam, K. S. J. Anderson, S. F. Anderson, J. Annis, N. A. Bah-



- call, I. K. Baldry, J. C. Barentine, A. Berlind, et al., *Astrophys. J. Supp.* **162**, 38 (2006), astro-ph/0507711.
- [25] I. Zehavi, D. J. Eisenstein, R. C. Nichol, M. R. Blanton, D. W. Hogg, J. Brinkmann, J. Loveday, A. Meiksin, D. P. Schneider, and M. Tegmark, *Astrophys. J.* **621**, 22 (2005), astro-ph/0411557.
- [26] D. J. Eisenstein, J. Annis, J. E. Gunn, A. S. Szalay, A. J. Connolly, R. C. Nichol, N. A. Bahcall, M. Bernardi, S. Burles, F. J. Castander, et al., *Astron. J.* **122**, 2267 (2001).
- [27] U. Seljak, A. Makarov, R. Mandelbaum, C. M. Hirata, N. Padmanabhan, P. McDonald, M. R. Blanton, M. Tegmark, N. A. Bahcall, and J. Brinkmann, *Phys. Rev. D* **71**, 043511 (2005).
- [28] J. F. Navarro, C. S. Frenk, and S. D. M. White, *Astrophys. J.* **462**, 563+ (1996).
- [29] C. Hirata and U. Seljak, *Mon. Not. R. Astron. Soc.* **343**, 459 (2003).
- [30] R. Mandelbaum, C. M. Hirata, U. Seljak, J. Guzik, N. Padmanabhan, C. Blake, M. R. Blanton, R. Lupton, and J. Brinkmann, *Mon. Not. R. Astron. Soc.* **361**, 1287 (2005), astro-ph/0501201.
- [31] R. Massey, C. Heymans, J. Bergé, G. Bernstein, S. Bridle, D. Clowe, H. Dahle, R. Ellis, T. Erben, M. Hettercheidt, et al., *Mon. Not. R. Astron. Soc.* **376**, 13 (2007), arXiv:astro-ph/0608643.
- [32] M. Davis, S. M. Faber, J. Newman, A. C. Phillips, R. S. Ellis, C. C. Steidel, C. Conselice, A. L. Coil, D. P. Finkbeiner, D. C. Koo, et al., in *Discoveries and Research Prospects from 6- to 10-Meter-Class Telescopes II. Edited by Guhathakurta, Puragra. Proceedings of the SPIE, Volume 4834, pp. 161-172 (2003)*. (2003), pp. 161–172.
- [33] R. K. Sheth and G. Tormen, *Mon. Not. R. Astron. Soc.* **308**, 119 (1999).
- [34] M. S. Warren, K. Abazajian, D. E. Holz, and L. Teodoro, *Astrophys. J.* **646**, 881 (2006), astro-ph/0506395.
- [35] J. S. Bullock, T. S. Kolatt, Y. Sigad, R. S. Somerville, A. V. Kravtsov, A. A. Klypin, J. R. Primack, and A. Dekel, *Mon. Not. R. Astron. Soc.* **321**, 559 (2001).
- [36] W. H. Press and P. Schechter, *Astrophys. J.* **187**, 425 (1974).
- [37] U. Seljak, A. Slosar, and P. McDonald, *Journal of Cosmology and Astro-Particle Physics* **10**, 14 (2006), astro-ph/0604335.
- [38] C. M. Hirata, R. Mandelbaum, U. Seljak, J. Guzik, N. Padmanabhan, C. Blake, J. Brinkmann, T. Budávári, A. Connolly, I. Csabai, et al., *Mon. Not. R. Astron. Soc.* **353**, 529 (2004).
- [39] J. Hartlap, P. Simon, and P. Schneider, *Astron. Astrophys.* **464**, 399 (2007), arXiv:astro-ph/0608064.
- [40] K. Pedersen and H. Dahle, *ArXiv Astrophysics e-prints* (2006), astro-ph/0603260.
- [41] R. Stanek, A. E. Evrard, H. Böhringer, P. Schuecker, and B. Nord, *Astrophys. J.* **648**, 956 (2006), astro-ph/0602324.
- [42] D. N. Spergel, R. Bean, O. Dore, M. R.olta, C. L. Bennett, G. Hinshaw, N. Jarosik, E. Komatsu, L. Page, H. V. Peiris, et al., *ArXiv Astrophysics e-prints* (2006), arXiv:astro-ph/0603449.
- [43] U. Seljak, A. Makarov, P. McDonald, S. F. Anderson, N. A. Bahcall, J. Brinkmann, S. Burles, R. Cen, M. Doi, J. E. Gunn, et al., *Phys. Rev. D* **71**, 103515 (2005).
- [44] M. D. Gladders and H. K. C. Yee, *Astron. J.* **120**, 2148 (2000).

- [45] U. Seljak, *Mon. Not. R. Astron. Soc.* **337**, 774 (2002), astro-ph/0203117.

## APPENDIX A: ANALYTIC COMPARISON OF EDDINGTON VERSUS MALMQUIST BIAS

Here, we analytically compare the magnitudes of Eddington and Malmquist biases with minimal assumptions for an analysis that proceeds as follows: determining the mass-observable relation from the lensing signal for the complete sample, and using the observed abundance with that mass normalization to constrain  $\sigma_8$ . Due to our strict cut in the observable, the steep decline of the mass function is going to (a) bias the average mass low (Malmquist bias) and (b) bias the abundance high (Eddington bias), whether the sample is flux- or volume-limited. We will now analytically prove our claim that the former effect dominates over the latter, leading to an underestimate of  $\sigma_8$ . We demonstrate this effect assuming a lognormal scatter in the mass-observable relation without placing a requirement on the size of the scatter.

The parameters of our analysis are the true cluster mass  $M$  and the estimate of the mass  $\tilde{M}$  derived from a cluster observable such as richness, X-ray luminosity, etc. Due to our use of a lognormal error distribution (i.e., constant relative rather than absolute scatter in the observable as a function of mass), our calculation uses the variables  $x = \ln(M/M_0)$  and  $\tilde{x} = \ln(\tilde{M}/M_0)$  for some arbitrary  $M_0$ . The relation between  $\tilde{x}$  and  $x$  is then

$$p(\tilde{x}|x) = \frac{1}{\sqrt{2\pi\sigma^2}} \exp[-(\tilde{x} - x)^2/2\sigma^2]. \quad (\text{A1})$$

We assume the halo mass function can be expressed as a summation over power laws, so we perform the calculations for a single power law and determine over what ranges of power law slope the calculation is valid. When using

$$\frac{dn}{dM} = \frac{n_0}{M_0} \left(\frac{M}{M_0}\right)^\alpha \quad (\text{A2})$$

we then find  $dn/dx = n_0 \exp[(\alpha + 1)x]$ .

### 1. Observed abundance calculation

First, we assume that the mass threshold is placed using the observable by requiring  $\tilde{x} > x_c$  for some  $x_c$ . The observed number density is then

$$n(\tilde{x} > x_c) = \int_{x_c}^{\infty} d\tilde{x} \int_{-\infty}^{\infty} dx \frac{dn}{dx} p(\tilde{x}|x) = \int_{x_c}^{\infty} d\tilde{x} \frac{d\tilde{n}}{d\tilde{x}} \quad (\text{A3})$$

where  $d\tilde{n}/d\tilde{x}$  is the observable mass function including effects of scatter. The integral over  $x$  can be performed

by completing the square to obtain

$$\begin{aligned} \frac{d\tilde{n}}{d\tilde{x}} &= n_0 \exp[(\alpha + 1)\tilde{x}] \exp[\sigma^2(\alpha + 1)^2/2] \\ &= \frac{dn(\tilde{x})}{dx} \exp[\sigma^2(\alpha + 1)^2/2] \end{aligned} \quad (\text{A4})$$

The latter term represents an increase in abundance due to scatter relative to the true halo mass function. Performing the integral over  $\tilde{x}$  in equation A3 for  $\alpha < -1$  (true for all mass ranges of interest in this paper) yields

$$\begin{aligned} n(\tilde{x} > x_c) &= \frac{n_0}{-(\alpha + 1)} \exp[(\alpha + 1)x_c] \exp[\sigma^2(\alpha + 1)^2/2] \\ &= n(x > x_c) \exp[\sigma^2(\alpha + 1)^2/2] \end{aligned} \quad (\text{A5})$$

The last factor in this equation represents the Eddington bias (which is always greater than unity) and shows that the observed abundance is higher than it would have been at the same threshold in the absence of scatter. This effect is stronger for a steeper mass function because, for a fixed scatter, there are even more lower mass halos to scatter into the sample when the mass function is steeper. If the scatter is ignored then this effect causes one to overestimate  $\sigma_8$  from the observed abundance.

## 2. True mean mass

We now compute the true mean mass of the sample, which must also be affected by the lower mass halos scattering into the sample. This is the mass that will be measured from the sample assuming the mass estimator is correct. Since we have assumed that the scatter in mass is lognormal, i.e. gaussian in  $x$ , we compute the average of  $x$  rather than of the mass itself,

$$\langle x \rangle = \frac{1}{n(\tilde{x} > x_c)} \int_{x_c}^{\infty} d\tilde{x} \int_{-\infty}^{+\infty} x \frac{dn}{dx} p(\tilde{x}|x) dx. \quad (\text{A6})$$

The integral over  $x$  can again be performed by completing the square, and after carrying out the integral over  $\tilde{x}$  we obtain

$$\langle x \rangle = x_c - \frac{1}{\alpha + 1} + (\alpha + 1)\sigma^2 = \langle \tilde{x} \rangle + (\alpha + 1)\sigma^2. \quad (\text{A7})$$

The first term  $\langle \tilde{x} \rangle$  is the estimated mean mass assuming our mass estimator. It equals the mean true mass in the absence of scatter. The final term represents the Malmquist bias; because  $\alpha + 1 < 0$ , scatter causes the estimated mean mass to be biased high relative to the true mean mass. Thus, if one neglected scatter, one would conclude from this sample that the mass estimator is biased and would apply a correction from equation A7 to rectify it, even though we have modeled the scatter between the estimated and true value of  $x$  as a gaussian

with zero mean. In the absence of an additional external calibration this is the only way to calibrate the estimator. While we have assumed that the mass estimator is given for every cluster in the sample, a random subsample of the complete sample would lead to the same result.

### a. Effects of ignoring scatter

We now consider the competition between the computed Malmquist and Eddington biases in an analysis that ignores the effects of scatter. From lensing, we see a mean mass given by equation A7 and determine an underestimated lower mass cutoff for our sample,

$$\hat{x}_c = x_c + (\alpha + 1)\sigma^2 < x_c. \quad (\text{A8})$$

Next, we compute the expected abundance for that lower mass cutoff assuming no scatter in the mass-observable relation, i.e.

$$\begin{aligned} n(x > \hat{x}_c) &= \int_{\hat{x}_c}^{\infty} dx \frac{dn}{dx} \\ &= \frac{n_0}{-(\alpha + 1)} \exp[(\alpha + 1)\hat{x}_c] \\ &= n(x > x_c) \exp[(\alpha + 1)^2\sigma^2] \end{aligned} \quad (\text{A9})$$

Finally, we compare the true observed abundance including scatter, equation A5, against the expected abundance in our analysis without scatter, equation A9. We find

$$\begin{aligned} \frac{n(\tilde{x} > x_c)}{n(x > \hat{x}_c)} &= \frac{\exp[\sigma^2(\alpha + 1)^2/2]}{\exp[\sigma^2(\alpha + 1)^2]} \\ &= \exp[-\sigma^2(\alpha + 1)^2/2] < 1. \end{aligned} \quad (\text{A10})$$

Thus, for an arbitrary size lognormal scatter in the mass-observable relation, the Malmquist bias dominates over the Eddington bias, leading us to underestimate  $\sigma_8$ . This conclusion is valid when the mass function can be expressed locally (near  $x_c$ ) as a power law in mass with slope steeper than  $-1$ , which is true for all masses of interest in this work and, indeed, in most typical cluster abundance analysis. As a demonstration, figure 5 shows  $\alpha$  (the power-law index of  $dn/dM$ ) for  $\Omega_m = 0.25$ ,  $\sigma_8 = 0.75$ ,  $z = 0.25$ , and  $n_s = 1.0$  for the mass ranges of interest, for which  $\alpha < -2$ . The bottom panel also shows the expected bias in  $\sigma_8$  as a function of lower mass cutoff for fixed  $\sigma = 0.1, 0.3$ , and  $0.5$  (no variation with mass) given the  $\alpha$  from the top panel and the change in predicted abundance with  $\sigma_8$  from figure 3. This bias arises due to the dominance of Malmquist bias leading to an apparent underestimate of number density, which is interpreted in an analysis without scatter as a suppression of  $\sigma_8$ .

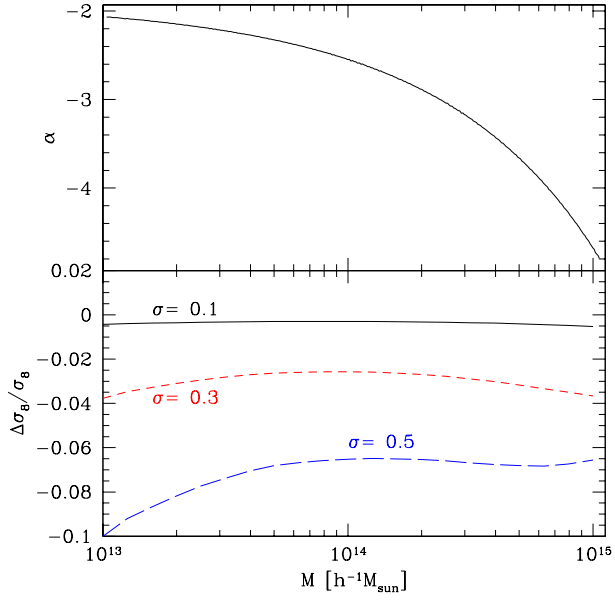


FIG. 5: Top panel: power law index of  $dn/dM$  for the mass range of interest for this work. Bottom panel: resulting bias in  $\sigma_8$  when ignoring scatter in the mass-observable relation at the 10%, 30%, and 50% level.